Vol 18 No 3, March 2009
1674-1056/2009/18(03)/1153-08

Chinese Physics B

© 2009 Chin. Phys. Soc.
and IOP Publishing Ltd

Electron temperature fluctuation in the HT-7 tokamak plasma observed by electron cyclotron emission imaging*

Xu Xiao-Yuan(徐小圆)[a)†], Wang Jun(王 俊)[a)], Yu Yi(余 弈)[a)], Wen Yi-Zhi(闻一之)[a)], Yu Chang-Xuan(俞昌旋)[a)], Liu Wan-Dong(刘万东)[a)], Wan Bao-Nian(万宝年)[b)], Gao Xiang(高 翔)[b)], N. C. Luhmann[c)], C. W. Domier[c)], Jian Wang(王 剑)[c)], Z. G. Xia(夏正刚)[c)], and Zuowei Shen(申作玮)[c)]

[a)] *Chinese Academy of Sciences (CAS) Key Laboratory of Plasma Physics, Department of Modern Physics, University of Science and Technology of China, Hefei* 230026, *China*

[b)] *Institute of Plasma Physics, Chinese Academy of Sciences, Hefei* 230031, *China*

[c)] *Department of Applied Science, University of California, Davis CA*95616, *USA*

(Received 7 June 2008; revised manuscript received 25 August 2008)

The fluctuation of the electron temperature has been measured by using the electron cyclotron emission imaging in the Hefei Tokamak-7 (HT-7) plasma. The electron temperature fluctuation with a broadband spectrum shows that it propagates in the electron diamagnetic drift direction, and the mean poloidal wave-number $\bar{k}_\theta$ is calculated to be about $1.58\,\mathrm{cm}^{-1}$, or $\bar{k}_\theta \rho_s \approx 0.34$. It indicates that the fluctuation should come from the electron drift wave turbulence. The linear global scaling of the electron temperature fluctuation with the gradient of electron temperature is consistent with the mixing length scale qualitatively. Evolution of spectrum of the fluctuation during the sawtooth oscillation phases is investigated, and the fluctuation is found to increase with the gradient of electron temperature increasing during most phases of the sawtooth oscillation. The results indicate that the electron temperature gradient is probably the driver of the fluctuation enhancement. The steady heat flux driven by electron temperature fluctuation is estimated and compared with the results from power balance estimation.

Keywords: electron temperature fluctuation, electron cyclotron emission imaging, Tokamak
PACC: 5225F, 5225G

1. Introduction

Particle and energy in a magnetic confinement tokamak plasma are not so well confined as predicted by many theories. Electrostatic fluctuation is considered to be most responsible for the anomalous transport. The heat flux driven by the fluctuation is given by

$$Q_\mathrm{e} = Q_{T_\mathrm{e}} + \frac{3}{2} T_\mathrm{e} \Gamma_\mathrm{e}, \tag{1}$$

where $Q_{T_\mathrm{e}} = 3/2 \left(n_\mathrm{e} \left\langle \tilde{T}_\mathrm{e} \tilde{E}_\theta \right\rangle / B \right)$ is the heat flux driven by the fluctuation of electron temperature and $\Gamma_\mathrm{e} = \left\langle \tilde{n}_\mathrm{e} \tilde{E}_\theta \right\rangle / B$ is the particle flux, with $\tilde{n}_\mathrm{e}$, $\tilde{T}_\mathrm{e}$ and $\tilde{E}_\theta$ representing the fluctuations in electron density, electron temperature and poloidal electric field, respectively. So far, only measurements of the density fluctuation $\tilde{n}_\mathrm{e}$ and the temperature fluctuation $\tilde{T}_\mathrm{e}$ in the interior of tokamak plasma have been obtained with a high spatial resolution by using different diagnostic techniques. The poloidal electrical field fluctuation $\tilde{E}_\theta$ lacks adequate sensitivity in measurement and is usually estimated from $\tilde{n}_\mathrm{e}$ based on Boltzmann relationship. Furthermore, the phase and the coherence between $\tilde{T}_\mathrm{e}$ and $\tilde{E}_\theta$ need to be simultaneously measured, however, they have not been measured simultaneously yet so far. Hence, only the upper limit estimation of Q_{T_e} in expression (1) can be obtained from $\tilde{n}_\mathrm{e}$ and $\tilde{T}_\mathrm{e}$ if a perfect correlation between them is assumed. The relationship between fluctuation and anomalous transport is understood only when $\tilde{n}_\mathrm{e}$, $\tilde{T}_\mathrm{e}$ and $\tilde{E}_\theta$ can be measured simultaneously.

The electron temperature fluctuation was mea-

*Project supported by the National Natural Science Foundation of China (Grant No 10335060), PRC–US Fusion Cooperation Program (Plasma Physics, Project A–5), and Chinese Academy of Sciences and Japanese Society of Promotion of Science (CAS-JSPS) Core University Program in Plasma and Nuclear Fusion.

†E-mail: xyxu3@mail.ustc.edu.cn

sured for the first time on the Texas Experimental Tokamak Upgrade (TEXT-U)[1] and Wendelstein 7-AS (W7-AS) stellarator[2] by using a technique correlated with the electron cyclotron emission (ECE). On TEXT-U the correlation radiometry of ECE (CRECE) correlates the emission of two largely overlapping sample volumes in two disjoint frequency bands to uncorrelated noise. They obtained a fluctuation level of about 1% for $\tilde{T}_e/T_e$. On W7-AS, the same ECE emitting plasma volume was observed by using two separated but identical radiometers. When the angle between them exceeded a minimum, the cross correlation function of the two radiometers uncorrelated the noise. The electron temperature fluctuation was at a level as low as about 0.5%. Experimental results obtained above show that a similar broadband spectrum feature covers over hundreds of kHz with the centre of the spectrum at about 50–100 kHz. The centre shift of the spectrum was also investigated and found to be dominated mainly by $E\times B$ rotation speed in the tokamak plasma.

The electron cyclotron emission imaging (ECEI) is an advanced two-dimensional ECE diagnostic technique with a spatial resolution of about 1 cm, better than the spatial resolution of conventional ECE radiometers particularly in the vertical direction. It can be used to measure the frequency as well as the wave number spectrum of the temperature fluctuation. The ECEI system has been developed and applied on the TEXT-U,[3] RTP,[4] the Toroidal Experiment for Technology Oriented Research (TEXTOR) tokamaks[5,6] as well as the Large Helical Device (LHD)[7] for the temperature fluctuation measurement. So far, an electron temperature fluctuation of about 1% has been found on tokamaks TEXT-U[1,8] and RTP.[9] By using the ECEI in TEXT-U, the poloidal wave number and statistical dispersion relation of temperature fluctuations in the core of the tokamak plasma were obtained, which accorded with theoretical calculations of the electron drift wave turbulence including a proper radial electric field.

In order to get an insight into the mechanism of the temperature fluctuation, the scaling of temperature fluctuation with ∇T_e has been investigated in most experiments. The experimental results show that the fluctuation amplitude increases in the radial direction in the core of plasma. The temperature fluctuation scales into $\tilde{T}_e/T_e \propto 1/\bar{k}_\theta L_{Te}$, which is the so-called mixing length scale predicted by most theories on the electrostatic transport.

The sawtooth is a periodic phenomenon, which is characterized by a sudden drop of the electron temperature in the plasma core region and a resulting ramp of the electron temperature outside the sawtooth inversion radius. The electron temperature gradient varies periodically with the sawtooth oscillation, which provides a way to have a deeper insight into the mechanism of temperature fluctuation. Temperature fluctuation due to the sawtooth heat pulse at high frequencies (about 50–250 kHz) was studied for the first time by using the CRECE on TEXT-U.[1,10] Similarly, density fluctuation due to the sawtooth oscillation was also found and studied on several other devices. The increasing of the density fluctuation due to the sawtooth heat pulse in the region with $q = 1$ radius has been found and studied by laser scattering experimentally on both the TFR (Tokamak Facility of Fontenay-aux-Roses) and Tore Supra tokamaks.[11,12] Moreover, a similar phenomenon was also found and studied in microwave scattering experiment on the TEXTOR.[13] The remainder of the present paper is organized as follows. In Section 2, the ECEI system setup is briefly described. Presented in Section 3 are the experimental results including the electron temperature fluctuation observed on HT-7, the scaling of electron temperature fluctuation with electron temperature gradient, and the energy transport. Finally, the findings of the present study are summarized in Section 4.

2. ECEI system setup

The experiment is performed on the HT-7 tokamak, which is a superconducting tokamak with a major radius of 1.22 m, a minor radius 0.27 m, and a circular poloidal limiter. The measurement reported herein takes place under the pure ohmic discharge at the following typical parameters: toroidal magnetic field $B_\varphi = 1.9$ T, plasma current $I_p = 150$ kA, central line-averaged density $\bar{n}_e = 1.9\times10^{19}\,\mathrm{m}^{-3}$, edge safety factor $q_a \approx 3.8$, $Z_{eff} \approx 4$, electron temperature $T_{eo} \approx 0.8$–1 keV and ion temperature $T_{io} \approx 0.35$–0.4 keV in the core. The electron temperature profile for a typical shot is shown in Fig.1. The profile is obtained by using three diagnostic techniques, i.e. the soft-x ray pulse height analyser (PHA) for measuring the temperature in a region of $r/a < 0.3$, the 16 channel heterodyne radiometer for ECE measurements, thereby mainly measuring the temperature in the high field side, and the ECEI for acquiring the

temperature information in the gradient region on the low field side. The relative electron temperature measured by the ECE radiometer and ECEI are multiplied with proper coefficients, respectively. The fitting result is $T_e = 0.94 \exp\{-[(\rho - \Delta\rho)/0.45]^2\}$ keV, where $\rho = r/a$ and $\Delta\rho = 0.01$. Studying the fluctuation indicated with the shading area in Fig.1 is the main point in this paper.

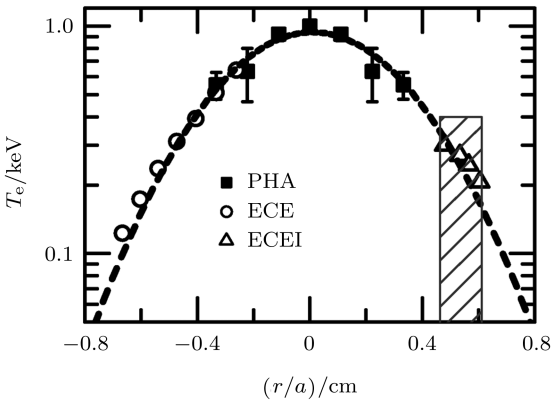


Fig.1. Profile of electron temperature T_e measured by using PHA, ECE and ECEI diagnostic techniques.

In the conventional ECE radiometry utilized is a single receiver located in the tokamak mid-plane to receive the ECE radiation, while used in the ECEI system are imaging arrays as the receiver/mixers. The second harmonic x-mode ECE radiations from distinct horizontal plasma chords pass through a specially designed lens system and focus onto each element of the detection imaging array, which is aligned along the vertical (E field) direction. Radiation at the same frequency is measured by using the ECEI system; hence the vertically aligned sample volumes at the same horizontal position in the plasma are diagnosed. The horizontal position of the sample volumes expressed in major radius can be derived from Ref.[14] and represented as $R \propto nB_0 f_{LO}$, where the harmonic number of the collected x-mode ECE radiation $n = 2$ in our case, B_0 is the magnetic field strength at the magnetic axis of the tokamak, and f_{LO} is the local oscillator (LO) frequency.

Figure 2 illustrates the ECEI system used on HT-7. The ECEI system is comprised of an imaging array with 16 detectors, some imaging lenses, a local oscillator and its power coupling optics, a signal processing electronic device and a data acquisition system. The horizontal position of the sample volumes can be scanned by changing the toroidal magnetic field or manually regulating the LO frequency (between 95 and 108 GHz) during discharges. Meanwhile, a good optical focus on the sample volumes can be obtained mainly by adjusting the location of the middle big imaging lenses in Fig.2. The details of the system can be found in Ref.[15] and will not be repeated here.

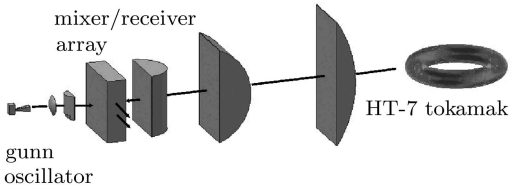


Fig.2. Schematic diagram of the ECE imaging system implemented on HT-7 tokamak.

The vertical positions of the individual horizontal sight lines and the beam patterns on the focal plane of the ECEI system have been measured in advance before its being mounted on HT-7.[15] In the vertical direction (E-plane), the spacing between neighbouring sample volumes is about 1.1 cm and the $1/e$ spot size of the individual horizontal sight lines is about 0.9–1.5 cm. Hence, the upper limit of the poloidal wave-number resolution $k_\theta = \pi/d_\theta$ for the system can be estimated to be about 2.1–3.5 cm^{-1}. In the horizontal direction, the sample volume size is restricted by the radio frequency bandwidth as well as the radiation bandwidth which arises from the magnetic field gradient, the Doppler broadening, and the relativistic broadening. The characteristic 1/e folding sample volume d_r is about 1 cm in that direction, i.e. $d_r \approx 1$ cm. Two-fixed-point correlation method is convenient and commonly used in estimating the wave-number spectrum of the fluctuation. The fluctuation in the plasma propagates from one point (x_1) to another point (x_2) with a separation $d = x_2 - x_1$ in between, which gives rise to the correlation between the fluctuation quantities measured at the two points. The quantities measured at the two points include fluctuation quantities and noise, which can be represented by $S_1 = \tilde{T}_{e1}(t) + \tilde{n}_1$ and $S_2 = \tilde{T}_{e2}(t) + \tilde{n}_2$, respectively. The relation between the fluctuation quantities is $\tilde{T}_{e2}(t) = \alpha \tilde{T}_{e1}(t - D)$, where D is the time delay between x_1 and x_2, and α is the attenuation factor due to the finite correlation length. The cross correlation function between the two points is given by $R_{S_1S_2(\tau)} = \int_{\infty}^{-\infty} S_1(t)S_2(t + \tau)\mathrm{d}t$. The radiation wave noises in S_1 and S_2, represented by $\tilde{n}_1$ and $\tilde{n}_2$, have much shorter correlation lengths, i.e. $R_{\tilde{n}_1\tilde{n}_2}(\tau) = 0$ and $R_{\tilde{n}_i\tilde{T}_j}(\tau)_{i\neq j} =$

0. Hence, correlation of the signals at the two points yields time-averaged fluctuation: $R_{S_1S_2(\tau)} = R_{\tilde{T}_{e1}\tilde{T}_{e2}} = \alpha\int_{\infty}^{-\infty}\tilde{T}_{e1}(t)\tilde{T}_{e1}(t+\tau-D)\mathrm{d}t$, which reaches a maximum value at a time delay of D. The cross power spectrum is given by $G_{12}(\omega) = \tilde{T}^*_{e1}(\omega)\tilde{T}_{e2}(\omega)$, which is related to correlation function by Fourier transform as $G_{12}(\omega) = \int_{\infty}^{-\infty}R_{S_1S_2}(\tau)\mathrm{e}^{-\mathrm{j}\omega\tau}\mathrm{d}\tau$. As a result, the cross power spectrum is obtained as $G_{12}(\omega) = \int_{\infty}^{-\infty}R_{S_1S_2}(\tau)\mathrm{e}^{-\mathrm{j}\omega\tau}\mathrm{d}\tau = \alpha|\tilde{T}_{e1}(\omega)|^2\mathrm{e}^{-\mathrm{j}\omega D}$ with $\tilde{T}_{e1,2}(\omega) = \int_{\infty}^{-\infty}\tilde{T}_{e1,2}(t)\mathrm{e}^{-\mathrm{j}\omega t}\mathrm{d}t$. The amplitude of cross power spectrum is $|G_{12}(\omega)| = \alpha\left|\tilde{T}_{e1}(\omega)\right|^2$, while the phase angle $\arg(G_{12}(\omega)) = -\omega D = -\omega d/v_{ph} = -k(\omega)d$ yields the propagating phase speed v_{ph}, the wave-number and the dispersion relations $k(\omega)$ of the fluctuation.[16]

3. Experimental results

3.1. Electron temperature fluctuation in HT-7

Figure 3 shows the $\tilde{T}_e$ cross power spectrum and the dispersion relation measured by the pair of the ECEI channels with a poloidal separation of 2.2 cm near the mid-plane at $r/a = 0.59$. The spectra are calculated by using the fast Fourier transform (FFT) technique with a frequency resolution of 7.8 kHz and ensemble averaging over more than 30,000 realizations by overlapping 50% for adjacent ensembles. They are comprised of the flat-top phases of five identical discharges of totally about 2 s. The statistical noise level of the power spectrum in Fig.3(a) and the error bars of k_θ in (b) are calculated from $\varepsilon[|\hat{G}_{xy}(f)|] = |G_{xy}(f)|/\gamma_{xy}(f)\sqrt{n_d}$ and $\Delta\hat{\varphi}_{xy} \approx \sin^{-1}([1-\gamma^2_{xy}(f)]^{1/2}/|\gamma_{xy}(f)|\sqrt{2n_d})$, where the estimation of the coherence function is represented by $\gamma_{xy}(f) = |G_{xy}(f)|\sqrt{G_{xx}(f)G_{yy}(f)}$, n_d is the number of ensemble averaging realizations and φ_{xy} is the phase angle of the cross power spectral density $G_{xy}(f)$.[17] The mean poloidal wave-number weighted by the power spectral density, $\bar{k}_\theta$, is calculated from 20 to 250 kHz to be 1.58 cm^{-1}, or $\bar{k}_\theta\rho_s \approx 0.34$. The fluctuation propagating in the electron diamagnetic direction and the wave-number estimation of about $\bar{k}_\theta\rho_s = 0.34$ (where $\rho_s = \rho_i(T_e/T_i)^{1/2}$, and $\rho_i = (m_iT_i)^{1/2}/eB$ is the ion Larmor radius) indicate that the fluctuation should be caused by the electron drift wave instability. Note that the cross power spectrum drops off near $f \approx 70$ kHz, causing a larger error of the wave-number, and then it rises again at higher frequencies. This may be caused by an aliasing effect at wavenumber $k_\theta = \pi/d \approx 1.5\,\mathrm{cm}^{-1}$, which is corresponding to $f \approx$70 kHz in Fig.3(b).

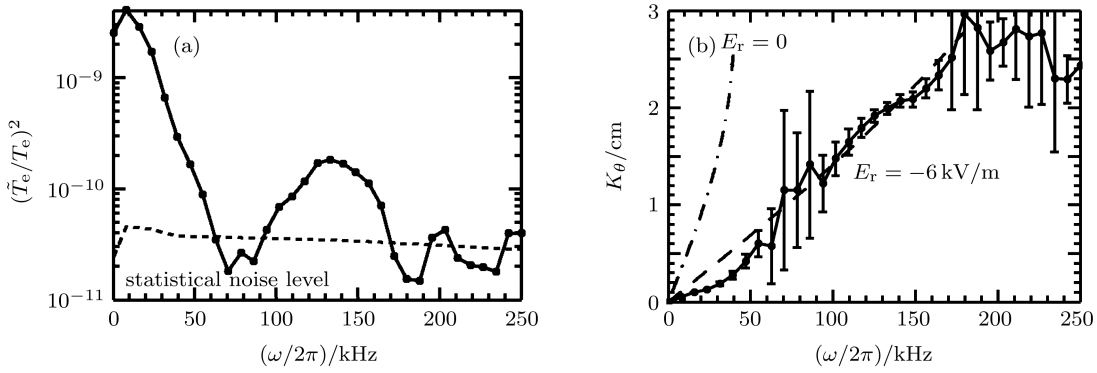


Fig.3. (a) Power spectral density and (b) statistical dispersion relation measured by a channel pairs with a poloidal separation of 2.2 cm near mid-plane at $r/a = 0.59$, under a pure Ohmic discharge with $I_p = 150$ kA and central line-averaged density $\bar{n}_e = 1.9\times10^{19}\,\mathrm{m}^{-3}$. The data are from shots 84295 to 84322.

For the electron drift waves, the dispersion relation is

$$\omega_k = \omega^*_e[1/(1+k^2_\theta\rho^2_s)] \quad (2)$$

where $\omega^*_e = k_\theta T_e/eBL_n$ and $L_n = -n_e(\mathrm{d}n_e/\mathrm{d}r)^{-1}$ that is the electron density scale length. The cold ions (i.e. $T_i = 0$) are assumed to be in this mode. The dash dotted curve in Fig.3(b) shows the dispersion relation as expressed in expression (2) where the electron density scaling length is about –0.1 m, and electron temperature is about 0.25 keV. However, the radial electric field gives rise to an $E\times B$ Doppler shift

of the mode frequency, i.e. $\omega = \omega_{\rm edw} + \omega_{E\times B}$. The modified drift wave dispersion relation with considering Doppler shift is shown as the long-dashed curve (see Fig.3(b)), which accords with the measurement line well from 0 to 170 kHz, indicating inward electric field $E_{\rm r} \approx -6\,{\rm kV/m}$. This value is reasonable since $E_{\rm r} \approx -4\,{\rm kV/m}$ was determined by heavy ion beam probe (HIBP) measurements of the plasma potential in TEXT-U.[18] Since the statistical dispersion relation is dominated mainly by the Doppler shift, thereby preventing the drift wave frequency from being identified, it provides a good estimation of the actual electric field.

Similar results are obtained, with the vertical location of the sample volumes moved from $r/a = 0.49$ to $r/a = 0.59$ by changing the magnetic field. The modification is that the mean phase speed decreases and the centre frequency for the broadband spectrum shifts toward lower frequencies. The mean phase speed $V_{\rm ph}$ and mean frequency $\bar{f}$ weighted by power spectrum from 100 to 250 kHz as a function of location are shown in Fig.4. As can be seen, $\bar{f}$ decreases from $r/a = 0.49$ to 0.59 in plasma with almost the same tendency as that of $V_{\rm ph}$. We can infer that the electric field becomes less negative outward in the plasma, and causes the Doppler shift to decrease, which is the dominant source of the centre frequency shift of the broadband spectrum.

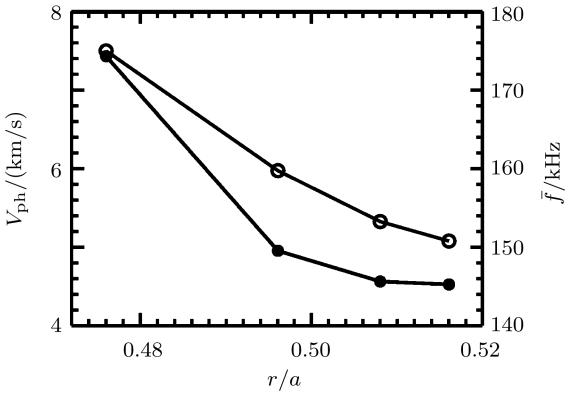


Fig.4. Mean phase speed $V_{\rm ph}$(solid circle) and mean frequency $\bar{f}$ (open circle) as a function of location, measured by the identical channel pair under the same discharge condition as that in Fig.2.

3.2. Scaling of $T_{\rm e}$ fluctuation with gradient $\nabla T_{\rm e}$

Many theories on the electrostatic transport predict that in the gradient region the temperature fluctuation should be scaled into so-called mixing length $\tilde{T}_{\rm e}/T_{\rm e} \propto 1/\bar{k}_\theta L_{T_{\rm e}}$, where $L_{T_{\rm e}}$ is the temperature gradient scale length. Plotted in Fig.5 is the fluctuation amplitude $\tilde{T}_{\rm e}/T_{\rm e}$ integrated over 20–250 kHz versus the temperature gradient $1/L_{T_{\rm e}}$. As can be seen, $\tilde{T}_{\rm e}/T_{\rm e}$ increases with $1/L_{T_{\rm e}}$ increasing according to the mixing length scale qualitatively. It indicates that the mechanism of temperature fluctuation is related to the gradient of temperature. To acquire more knowledge about the mechanism of temperature fluctuation, the evolution of the temperature fluctuation during the sawtooth oscillation is investigated.

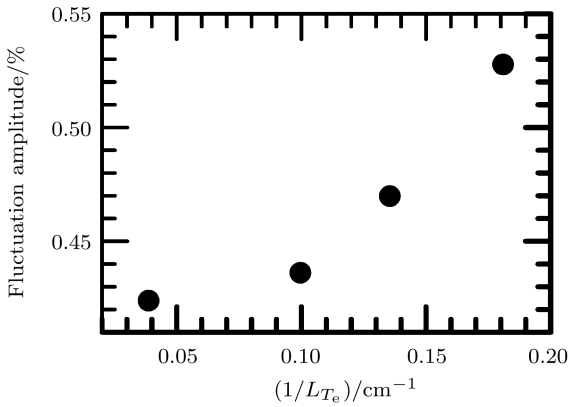


Fig.5. Relationship of temperature fluctuation amplitude with electron temperature gradient $1/L_{T_{\rm e}}$ under the same discharge condition as that in Fig.3.

The sawtooth oscillation is characterized by a periodic fast heat loss in the core plasma region. In the core, the electron temperature ramps up slowly in most of the sawtooth period while crashes down quickly in the remainder. The crash transports the heat out, thus the temperature outside the core ramps up quickly and then drops off slowly as the heat is dissipated. The electron temperature fluctuation at high frequencies, rising prominently due to the sawtooth heat pulse propagating outside the core, was found and studied for the first time by CRECE on TEXT-U.[1,10] The data there are subdivided into 8 bins representing different phases of the oscillation. All phases are relative to the local discontinuous rise in electron temperature at the measurement location. The data in each phase bin is Fourier analysed to produce the time-averaged cross power spectrum for each sawtooth phase. Successive sawtooth phases are treated similarly, and the spectrum of each sawtooth phase is ensemble averaged over many sawtooth oscillations to obtain the requisite statistics. To study the fluctuation due to the heat pulse in HT-7, a similar method

is used except for some differences shown below. Sawtooth phases are divided according to the discontinuous change in soft-x ray sawtooth signal in the plasma core region. As irregular sawtooth periods may bring about more noises, the sawtooth oscillations with periods exceeding ±5% of the mean sawtooth period that is about 2.2 ms are discarded.

Figure 6 depicts the evolution of cross power spectrum of the temperature fluctuation outside inversion radius under the same discharge condition as that of Fig.3. Each sawtooth phase spectrum incorporates about 50 sawtooth oscillations representing an average time of 100 ms. The convention indicated in Fig.6(a) shows the sawtooth phases. The phases are labelled with capitals from A to H, where A represents the crash phase while H represents the phase just before the next crash. In Fig.6(a), only the spectra of the four typical phases: A, C, E and G are shown. The statistical noise level represented with dashed line is calculated according to mean $(A-H)$ data. From a comparison among the spectra of the four phases, we can easily see a prominent broad spectrum between about 100 and 170 kHz at phase C.

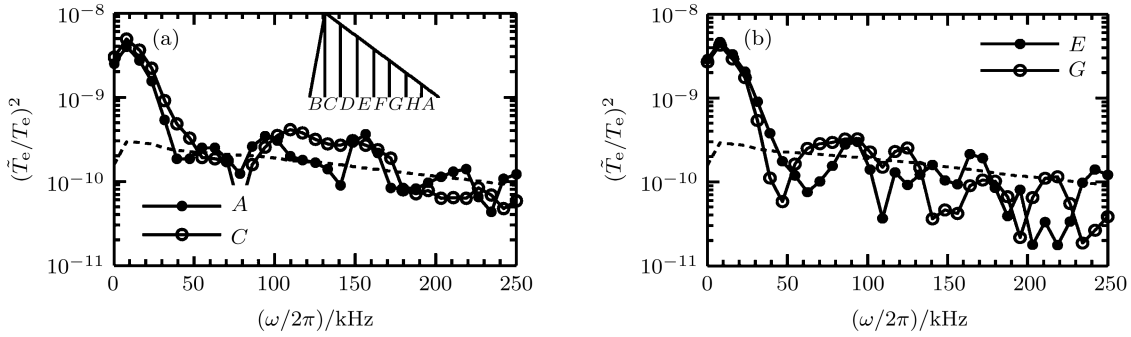


Fig.6. Evolutions of the spectrum of temperature fluctuation during a sawtooth oscillation under the same discharge condition as that in Fig.3. Here only the spectra of 4 typical phases A and C (a), E and G (b) are shown, and the statistical noise level represented with dashed lines is calculated by averaging the data from A to H.

In order to understand the turbulence enhancement, the relation between integrated fluctuation and temperature gradient $1/L_{T_e}$ during the eight phases is studied (Fig.7). The value of $1/L_{T_e}$ for each phase is an average over corresponding parts of all the sawtooth oscillations. As shown in Fig.7, as the heat pulse propagates outside the inversion radius initially, the temperature gradient increases quickly from A to C, and the fluctuation magnitude also increases. As the heat pulse is dissipated, the temperature gradient drops off slowly from phases C to G, while the fluctuation magnitude reduces almost linearly with the temperature gradient decreasing. The steepest temperature gradient in phase C corresponds to the highest fluctuation magnitude. In Fig.7, the temperature fluctuation increases with the temperature gradient increasing during most phases of the sawtooth oscillations. It indicates that the temperature gradient is probably the driver of the turbulence enhancement.

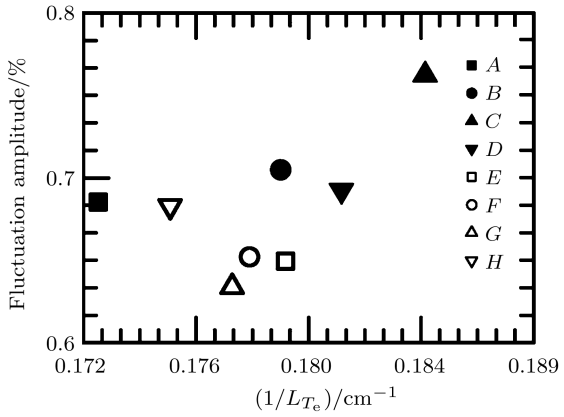


Fig.7. Relationship between fluctuation amplitude and temperature gradient during 8 sawtooth phases corresponding to the case of Fig.6, where the amplitude is obtained by integrating the fluctuation spectrum between 20–250 kHz.

If we compare Fig.5 and Fig.7, it seems that they are contradictive: in the global scaling of $\tilde{T}_e/T_e$ versus $1/L_{T_e}$, the fluctuation is enhanced a little for a large increment in temperature gradient, while during the sawtooth oscillation, on the contrary, the fluctuation rises significantly for a small increment in temperature gradient. It seems that the fluctuation enhancement during the sawtooth crash is related to the profile resilience, above which a small change in temperature

profile will lead to a tremendous increase in fluctuation amplitude to restabilize the profile.

3.3. Energy transport

In order to understand the relationship between fluctuation level and heat transport, the maximum heat flux resulting from the measured temperature fluctuation should be compared with the heat flux estimated from the power balance consideration. The maximum of the electrostatic fluctuation driven electron heat flux containing $\tilde{T}_e$ can be derived from the first term in expression (1)[19]

$$Q_{T_e} = \frac{3}{2}\frac{n_e\left\langle \tilde{T}_e\tilde{E}_\theta \right\rangle}{B_\varphi} = \frac{3}{2}\frac{\bar{k}_\theta n_e T_e^2}{eB_\varphi}\frac{e\tilde{\varphi}}{T_e}\frac{\tilde{T}_e}{T_e}, \qquad (3)$$

where the ensemble average $\langle\ \rangle$ is replaced by the root mean square (RMS) value of the fluctuations on the assumption that the phase angle between $\tilde{T}_e$ and $\tilde{E}_\theta$ is zero for maximum heat flux. If the ratio $e\left|\tilde{\phi}\right|/T_e$ is 1% similar to that in TEXT-U,[19] $\overline{k}_\theta \approx 1.58$ the same as that mentioned in Section 3.1, and $\tilde{T}_e/T_e$ is estimated to be 0.54% as a maximum fluctuation level, then the maximum heat flux expressed by expression (1) gives about $1.2\,\mathrm{kW/m^2}$ from the measured temperature fluctuation in HT-7. It is much smaller than the heat flux $Q_e \approx 11\,\mathrm{kW/m^2}$ estimated from the power balance consideration. The difference between Q_{T_e} and Q_e could be caused mainly by the contribution of the convected heat flux [the second term in expression (1)]. Moreover, the estimation of $\overline{k}_\theta$, T_e and $e\left|\tilde{\phi}\right|/T_e$ may induce a variation in predicted maximum heat flux expressed by expression (1).

4. Summary

A magnitude of electron temperature fluctuation, as low as about 0.5%, is found by ECEI on HT-7 tokamak. The fluctuation with a broad spectrum propagates in the electron diamagnetic drift direction. The mean poloidal wave-number is calculated to be $\bar{k}_\theta\rho_s \approx 0.34$. These results reveal that the fluctuation is due to the electron drift wave turbulence. The spectrum drops off near $f \approx 70\,\mathrm{kHz}$, resulting in a larger error of the wave-number, and then rises again at higher frequencies, which is probably caused by an aliasing effect. The frequency shift of the high-frequency broad mode shows a tendency almost the same as that of the variation in phase speed when the horizontal location of the sample volume moves outward. It indicates that the frequency shift is due mainly to the Doppler shift.

The fluctuation magnitude shows linear scaling with the gradient of electron temperature, which is consistent with the mixing length scale qualitatively. Moreover, the temperature fluctuation increases with the electron temperature gradient increasing during most phases of the sawtooth oscillations. These results indicate that the gradient is probably the driver for enhancing the turbulence. The electron heat flux driven by the maximum temperature fluctuation is found to be much lower than the heat flux obtained from the power balance consideration. It could come mainly from the contribution of the convected heat flux.

Acknowledgment

The authors thank the HT-7 group for their great help .

References

[1] Watts C, Gandy R F, Cima G, Bravenec R V, Ross D W, Wootton A J, Ouroua A, Heard J W, Crowley T P, Schoch P M, Brower D L, Jiang Y, Deng B, Domier C W and Luhmann N C 1996 *Phys. Plasmas* **3** 2013

[2] Sattler S, Hartfuss H J and W7-AS Team 1994 *Phys. Rev. Lett.* **72** 653

[3] Deng B H, Burns S R, Domier C W, Hillyer T R, Hsia R P, Luhmann N C, Brower D L, Cima G, Donne A J H, Oyevaar T and RTP Team 2001 *Fusion Eng. Des.* **53** 77

[4] Deng B H, Hsia R P, Domier C W, Burns S R, Hillyer T R, Luhmann N C, Oyevaar T and Donne A J H 1999 *Rev. Sci. Instrum.* **70** 998

[5] Wang J, Domier C W, Xia Z G, Liang Y, Luhmann N C, Park H, Munsat T, Mazzucato E, van de Pol M J, Classen I G J and Donne A J H 2004 *Rev. Sci. Instrum.* **75** 3875

[6] Deng B H, Domier C W, Luhmann N C, Donne A J H and van de Pol M J 2001 *Rev. Sci. Instrum.* **72** 368

[7] Mase A, Kogi Y, Kawahata K, Nagayama Y, Luhmann N C, Deng B H, Domier C W, Mazzucato E, Munsat T and Park H K 2003 *Fusion Eng. Des.* **43** 237

[8] Deng B H, Brower D L, Cima G, Domier C W, Luhmann N C and Watts C 1998 *Phys. Plasmas* **5** 4117

[9] Deng B H, Domier C W, Luhmann N C, Brower D L, Donne A J H, Oyevaar T and van de Pol M J 2001 *Phys. Plasmas* **8** 2163

[10] Watts C and Gandy R F 1995 *Phys. Rev. Lett.* **75** 1759

[11] Gervais F, Hennequin P, Quemeneur A, Truc A, Pecquet A L, Laviron C and Devynck P 1997 *Plasma Phys. Control Fusion* **39** 43

[12] Andreoletti J, Laviron C, Olivain J, Pecquet A L, Gervais F, Gresillon D, Hennequin P, Quemeneur A and Truc A 1991 *J. de Physique* III **1** 1529

[13] Jadoul M, Waidmann G and Vandenplas P E 1998 *Plasma Phys. Control Fusion* **40** 381

[14] Wang J, Wen Y Z, Yu C X, Wan B N, Luhmann N C, Wang J and Xia Z G 2004 *Plasma Sci. Technol.* **6** 2166

[15] Wang J, Xu X Y, Wen Y Z, Yu C X, Wan B N, Luhmann N C, Wang J and Xia Z G 2006 *Plasma Science Technol.* **8** 76

[16] Deng B H 1999 *Two Dimensional Electron Cyclotron Emission Imaging Study of Electron Temperature Profiles and Fluctuations in Tokamak Plasmas* Ph.D. dissertation, University of California, Davis

[17] Bendat J S and Piersol A G 1986 *Random Data: Analysis and Measurement Procedures* (New York: Wiley) p267 & p281

[18] Bravenec R V 1992 *Phys. Fluids* B **4** 2127

[19] Cima G, Bravenec R V, Wootton A J, Rempel T D, Gandy R F, Watts C and Kwon M 1995 *Phys. Plasmas* **2** 720